Viscous stabilization of drying front: three-dimensional pore network simulations

T. Metzger, E. Tsotsas

Thermal Process Engineering, Otto-von-Guericke-University, P.O. 4120, D-39016 Magdeburg, Germany

Abstract

In this study, a recently developed pore network drying model (Metzger et al. 2007a), which accounts for liquid viscosity, is applied to three dimensions for the first time. Isothermal convective drying is simulated for a cubic network (25×25×50) with pore throats of mono-modal radius distribution. The role of liquid viscosity is assessed by comparison with non-viscous drying of the same network. Simulation results are presented as phase distributions, saturation profiles and drying rate curves.

Keywords: capillary porous media, phase distributions, drying rate curves, viscosity

1. Introduction

Pore network models are a suitable tool to examine the role of pore-scale transport phenomena and pore structure on the processing behaviour of porous media. During the past one and a half decades, several research groups have applied pore network modelling to drying of capillary porous media, continuously adding new transport phenomena and increasing network size.

In network models, the porous medium is represented by a network of interconnected pores which have a prescribed geometry (cylindrical in our study) but are random in their size. Our model approach is based on the work of Prat (1993) who interpreted the drying process as an invasion percolation driven by evaporation. At every moment of the process, the largest pore at the gas-liquid interface empties because its meniscus can produce the highest liquid pressure. Due to the random spatial distribution of pore size, the liquid phase typically splits up into numerous clusters that may be temporarily trapped, but eventually all liquid will evaporate. The time scale of the process is given by vapour diffusion in the empty regions of the network.

In this isothermal model, capillary flow is only determined by the spatial distribution of pore size. However, if other effects like gravity, liquid viscosity or non-uniform temperature play a role, drying behaviour can differ significantly. The model extension to gravity is straightforward by allocating to each pore a potential which then determines the order of invasion (Prat 1993). If the network dries out from the

top, gravity has a stabilizing effect on the drying front. Laurindo and Prat (1996) performed experiments with two-dimensional micro models which nicely confirmed the simulated phase patterns as well as their modification due to gravity.

Recently, the stabilizing effect of gravity has also been studied in three dimensions by Yiotis et al. (2006) who simulated drying of an 80×80×80 network. However, if gravity plays no role and lateral diffusion in the gas-side boundary layer is modelled, a constant drying rate period is obtained. Such computationally intensive three-dimensional network simulations are important, because the additional dimension leads to less trapping (see also Le Bray and Prat 1999).

Prat and Bouleux (1998) predicted a stabilization of the drying front if liquid viscosity must be accounted for (i.e. for large networks of small pores with a narrow size distribution); however, they only performed stationary simulations. Other researchers have included viscous effects into their (two-dimensional) pore network models, but the effect of liquid viscosity on drying kinetics and phase distributions has never been studied systematically: Nowicki et al. (1992) were interested in effective parameters and did not report on phase distributions and drying rates at the sample scale; and Yiotis et al. (2001) simulated drying of porous rock when gas is purged through large fractures and viscous effects mainly play a role in the gas phase.

In the present work, we investigate the viscous stabilization of the drying front for a three-dimensional network and its effect on the drying rate curve. We will point out the special character of this stabilization: whereas in the gravity-stabilized case the front width is constant throughout the drying process, viscous effects depend on the current flow rates so that the drying front can widen up during the process.

It is worth mentioning that temperature gradients can also lead to a stabilization of the drying front (Plourde and Prat 2003) and that pore structures with a bimodal pore size distribution may show very different drying behaviour (e.g., Metzger et al. 2007a). In the present work, we restrict ourselves to isothermal drying of mono-modal structure.

2. Drying model

In the following, the main concepts of non-viscous and viscous network drying model are recalled (for more details refer to Metzger et al. 2007b).

2.1. Non-viscous model

The cubic pore network is built from cylindrical pore throats with radii r_{ij} obeying a normal number distribution. Initially, the network is fully saturated with water. During drying, it is open for evaporation at the top whereas the bottom is closed and the sides are connected for periodic boundary conditions in horizontal directions. Vapour transfer to the dry air flow is modelled by diffusion through a boundary layer of uniform thickness which is discretized by extending the nodes of the network. In the gas phase (dry part of network and boundary layer), quasi-steady vapour diffusion between two nodes is described by

$$\sum_j \dot{M}_{v,ij} = \sum_j A_{ij} \frac{\delta}{L} \frac{p\widetilde{M}_v}{\widetilde{R}T} \cdot \ln\left(\frac{p - p_{v,i}}{p - p_{v,j}}\right) = 0 \qquad (1)$$

2

where L is distance between nodes, A_{ij} exchange area (πr_{ij}^2 for network, L^2 for boundary layer), $\widetilde{M}_v$ molar vapour mass, $\widetilde{R}$ universal gas constant, p gas pressure, T absolute temperature and $p_{v,i}$ vapour pressure. The system of equations (1) is solved by applying the vapour pressure of drying air at the top edge of the boundary layer and saturation vapour pressure next to the gas-liquid interface. (Neither adsorption and liquid films nor Knudsen and Kelvin effects are modelled.)

Concerning the liquid-filled part of the network, random pore size distribution and capillary flow lead to irregular emptying of pores and the appearance of disconnected clusters. If viscous (and gravity) effects are neglected, water flow within these liquid clusters is entirely controlled by capillary pressure differences so that the largest meniscus throat of the cluster empties at the evaporation rate of the whole cluster. Time stepping is given by complete emptying of one throat since this will change liquid connectivity as well as the set of equations (1) for vapour diffusion.

2.2. Viscous model

If liquid viscosity is accounted for, liquid flow rates depend on actual pressures $p_{w,i}$ and at each liquid pore node add up to zero as

$$\sum_j \dot{M}_{w,ij} = \sum_j \frac{\pi r_{ij}^4}{8 \nu_w L_{ij}} \left(p_{w,i} - p_{w,j} \right) = 0 \qquad (2)$$

where ν_w is kinematic viscosity of water and L_{ij} liquid-filled length of pore throats. Boundary conditions to equations (2) are given at the menisci at the liquid-gas interface. For stationary menisci (in full throats where liquid can be provided at the local evaporation rate), the second kind boundary condition $\dot{M}_{w,ij} = \dot{M}_{v,ij}$ is applied.

For moving menisci (in the largest throat of the cluster, in all partially filled throats and where liquid cannot be supplied at the local evaporation rate), the boundary condition of first kind $p_{w,j} = p - 2\sigma/r_{ij}$ (with surface tension σ) is used. Since choice of boundary conditions and flow rates are interdependent, iteration is used to determine the actual liquid flow field. The motion of menisci is obtained as the difference between vapour and liquid flow, and the same principle of time stepping is applied as in the non-viscous case. (Note that, in the gas phase, viscosity is not modelled and constant pressure is assumed.)

3. Simulation results

Present computational limitations impose a relatively small network size (25×25×50) so that rather unrealistic values have to be chosen for pore geometry and drying conditions to observe significant viscous effects. Air flow is at room temperature and absolutely dry; boundary layer is 50 µm thin, corresponding to a mass transfer coefficient $\beta = 0.51$ m/s. Throats have a very narrow radius distribution (50 ± 1 nm) and length 500 nm; this means that porosity is low (9.4 %) and that only a thin near-surface region of the porous medium is described. Effects similar to the ones discussed below will also occur for realistic conditions, but over longer distances.

Being interested in the role of liquid viscosity, drying of the same network is once simulated neglecting the viscous effects and once accounting for them. Respective
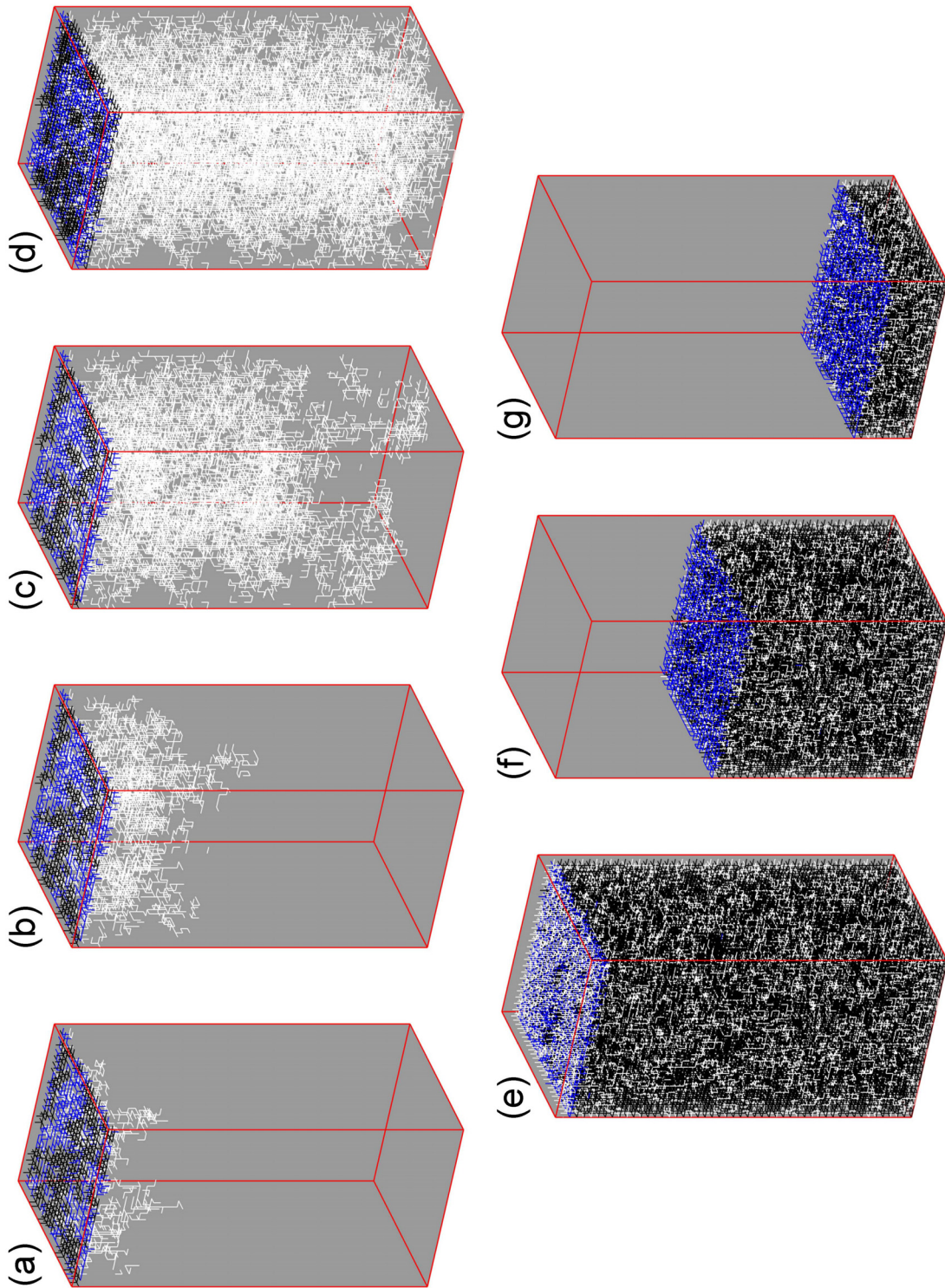
Figure 1: Phase distributions for *non-viscous* case at network saturations (a) 0.98 (b) 0.95 (c) 0.86 (d) 0.75 (e) 0.67 (f) 0.39 (g) 0.11; white lines represent empty throats, black is for liquid throats and blue for partially filled throats. The network is open for evaporation at the top, periodic boundary conditions are applied in horizontal directions. (For better readability, empty throats are not shown in top layers with an average saturation lower than 0.26; neither are full throats shown in bottom layers with an average saturation higher than 0.74.)
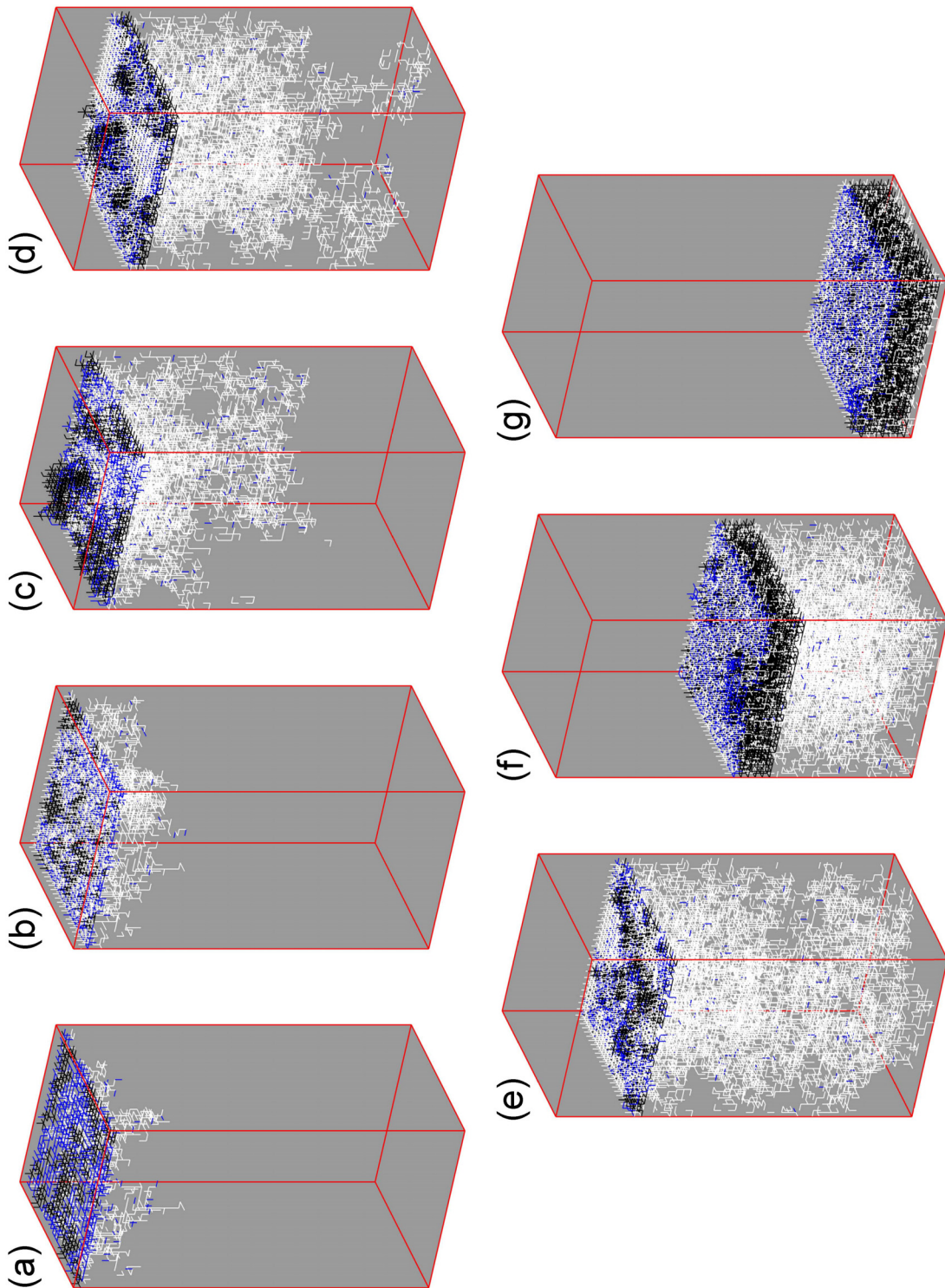
Figure 2: Phase distributions for *viscous* case at network saturations (a) 0.98 (b) 0.95 (c) 0.86 (d) 0.75 (e) 0.67 (f) 0.39 (g) 0.11; white lines represent empty throats, black is for liquid throats and blue for partially filled throats. The network is open for evaporation at the top, periodic boundary conditions are applied in horizontal directions. (For better readability, empty throats are not shown in top layers with an average saturation lower than 0.26; neither are full throats shown in bottom layers with an average saturation higher than 0.74.)
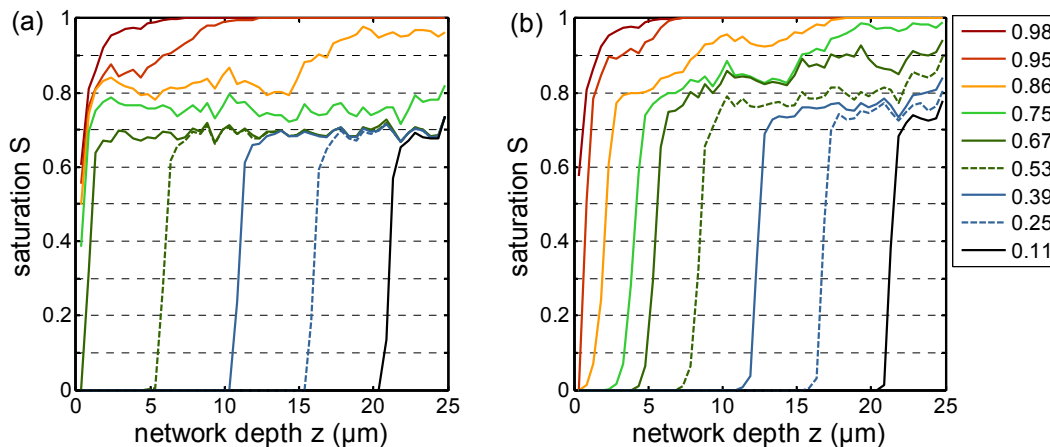
Figure 3: Profiles of slice-averaged saturation during drying: (a) non-viscous (b) viscous.
(Solid lines correspond to the choice of phase distributions shown in Figures 1 and 2.)
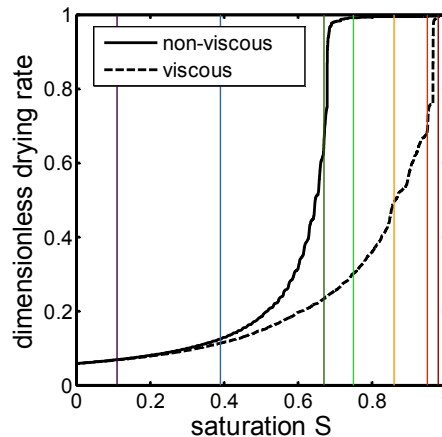

Figure 4: Drying rate curves for non-viscous and viscous case.
(Vertical lines correspond to the choice of network saturations in the other figures.)

phase distributions during drying are shown in Figures 1 and 2; by slice-averaging, they are converted into one-dimensional saturation profiles as plotted in Figure 3. Corresponding drying rate curves are given in Figure 4.

If liquid viscosity is neglected, capillary pumping experiences no constraint as long as the liquid is connected over the whole network. During this period, no drying front occurs, but gas penetrates into the depth of the network and saturation level drops more or less uniformly throughout the network (Figures 1a-d and 3a). Network surface stays sufficiently wet so that lateral vapour transfer in the gas-side boundary layer can ensure that liquid is evaporated at a constant rate (Figure 4). At a critical saturation of about 0.7, the liquid phase has split up into small disconnected clusters, network surface dries out (Figure 1e) and a receding evaporation front is observed (Figures 1f-g and 3a). Drying rate drops due to the additional vapour transfer resistance in the network (Figure 4). The mentioned critical saturation is lower for larger pore networks (Le Bray and Prat 1999, Yiotis et al. 2006).

If viscous effects are modelled, they do not play a significant role in the very initial drying phase (here S > 0.98) which is still dominated by capillary forces (compare Figures 1a and 2a). But as flow distances become longer and surface saturation decreases, differences in capillary pressure are not enough to supply liquid at the high local evaporation rates (even enhanced by lateral diffusion in the boundary layer). Therefore, all surface throats dry out (Figure 3b) and a quite narrow drying front recedes into the pore network. As a consequence, drying rates are strongly reduced (Figure 4), so that, as drying proceeds, this receding front can widen up gradually (Figures 2c-d and 3b). In the viscous case, breakthrough occurs long after network surface is dry. Note also that the competition between menisci for liquid flow is documented by many moving menisci in one cluster (blue throats in Figure 2).

With further decreasing drying rate, saturation gradient is reduced more and more (Figure 3b) and local saturations approach the limit for liquid disconnection (Figures 2e-f). In the final stages of drying, viscous effects play only a little role (compare Figures 1g and 2g, see Figure 4). This non-viscous limit ought to gain significance for deeper networks.

4. Conclusions

We have observed that viscous effects mainly play a role in the intermediate stages of drying whereas short-time and long-time drying behaviour are similar to the non-viscous case. The relative size of viscous effects is decisive for phase distributions and drying rates in these intermediate stages of the drying process – and will especially determine the duration of the constant drying rate period.

Future work shall further investigate the local variation of saturation in the drying front and the scaling behaviour of its width with capillary number as already studied by Prat and Bouleux (1999). This shall pave the way to describe drying behaviour of much larger porous structures.

In the same context, a continuous model shall be assessed that accounts for vapour diffusion in a dry zone and for viscous flow in the partially saturated zone driven by differences in capillary pressure (described by the generalized Darcy law). To this purpose, effective model parameters will first be computed from the phase distributions as observed in a drying pore network; then, the evolution of continuous saturation profiles shall be compared to profiles obtained from network simulations (as in Figure 3b).

References

Laurindo, J.B. and Prat, M., (1998) *Drying Technology* 16, 1769-1788.
Le Bray, Y., and Prat, M., (1999) *Int. J. Heat Mass Transfer* 42, 4207-4224.
Metzger, T., Irawan, A. and Tsotsas, E., (2007a) *Drying Technology* 25, 49-57.
Metzger, T., Tsotsas, E., Prat, M., Ch. 2 in: Tsotsas, E., Mujumdar A.S., (Eds.), *Modern Drying Technology 1: Computational Tools at Differents Scales.* Wiley, in print (2007b).
Nowicki, S.C., Davis, H.T., Scriven, L.E., (1992) *Drying Technology* 10, 925-946.
Plourde, F., and Prat, M., (2003) *Int. J. Heat Mass Transfer* 46, 1293-1307.
Prat, M., (1993) *Int. J. Multiphase Flow* 19, 691-704.
Prat, M., and Bouleux, F., (1999) *Phys. Rev. E* 60, 5647-5656.
Yiotis, A.G., Stubos, A.K., Boudouvis A.G., and Yortsos Y.C., (2001) *Adv. Water Resour.* 24, 439-460.
Yiotis, A.G., Tsimpanogiannis, I.N., Stubos A.K., Yortsos, Y.C., (2006) *J. Colloid Interface Sci.* 297, 738-748.